Analysis of Detector Response Using 3-D Position-Sensitive CZT Gamma-Ray Spectrometers

Feng Zhang, *Student Member, IEEE*, Zhong He, *Senior Member, IEEE*, and Dan Xu

***Abstract*—Two 2.25-cm^3 CdZnTe gamma-ray spectrometers with three-dimensional (3-D) position sensitivity were constructed and tested. By using 11 × 11 pixellated anodes and depth-sensing techniques, individual spectral data for each of ∼4800 voxels were collected throughout the detector volume. Energy resolution of 1.11% and 1.14% FWHM at 662 keV were obtained for single-pixel events from these two detectors, respectively. Spatial variations of electron mobility-lifetime product, energy resolution, photopeak efficiency, and total efficiency have been observed and analyzed. This analysis provides a direct observation on the uniformity of detector response (due to material, weighting potential, and electric field distribution) in 3-D. Possible defects in the detector are identified. The impact of the spatial variation of detector response on a CZT gamma-ray spectrometer is discussed.**

***Index Terms*—CdZnTe, CZT, gamma-ray spectroscopy, ionization energy, position sensitive, spectrometer, trapping, weighting potential.**

I. Introduction

THE spectroscopic performance of large volume CdZnTe room temperature gamma-ray detectors has been greatly improved using the three-dimensional (3-D) single polarity charge-sensing technology [1]–[6]. However, detector material nonuniformity and electron-trapping variation along the lateral direction can still degrade the energy resolution. The 3-D position-sensitive CdZnTe gamma-ray spectrometers allow us to study directly the variation of 3-D detector response down to the limit of the position resolution (1.27 × 1.27 mm in lateral direction and 0.25 mm in depth at 662 keV) over the whole detector volume.

Two identical 3-D position-sensitive CdZnTe detectors (#2.2 and #2.3) were fabricated by eV-Products [7]. Each $1.5 \times 1.5 \times 1.0$ cm^3 detector employs 11 × 11 pixellated anodes and a conventional planar cathode. The cathode and the 121 anode pixels were wire bonded to and read out through the VAS2/TAT2 ASICs developed by Ideas ASA [8]. Detailed information about the detectors and the electronics can be found in another paper of our group [6]. Both detectors were irradiated by an uncollimated 10 μCi ^{137}Cs gamma-ray point source located 5 cm from the cathode surface. The pixel location provides the interaction's lateral coordinates, while the ratio of the cathode to anode signals (C/A ratio) [9], [10] and the electron drift time [3]–[6] are both used to obtain the interaction depth.

Since this study focuses on the spatial variations in the detector response, only single-pixel events are analyzed. Although both the C/A ratio and the electron drift time can be used for single-pixel events, due to limited timing resolution (∼40 ns), the depth resolution using the electron drift time was estimated to be ∼0.8 mm. The C/A ratio depth-sensing method achieved ∼0.25-mm depth resolution at 662 keV and, thus, was chosen for this study. This 3-D position-sensing technique divides the whole volume of the detector into $11 \times 11 \times 40$ voxels. Individual spectra from each voxel can be retrieved from these 3-D-CZT spectrometers [1]. The effects on photopeak centroids, photopeak counts, and energy resolution due to electron trapping, ionization energy, and weighting potential can then be studied down to the limit of the position resolution. Such analysis of the 3-D detector response can be used to identify possible defects in the detector and to assess the quality of the crystal and the detector fabrication.

II. Electron Trapping

When a gamma ray interacts inside a CdZnTe detector, electron-hole pairs are generated. Since the cathode is biased at −2000 V and the anode pixels are at virtual ground, the electrons drift toward the anode, while the holes drift toward the cathode. Because of their poor mobility and lifetime, the holes do not contribute to the signals during the 1 μs electron collection time. The signals on both the cathode and the anode pixel are only dependant on the movement and collection of the electrons. Due to the small pixel effect [11], the signal on the anode pixel is nearly independent of the interaction depth and only proportional to the number of electrons collected, while the signal on the cathode is dependent on the interaction depth. Thus, for single-pixel events, the ratio of the cathode signal to the anode signal can be used to determine the interaction depth [12]. However, the C/A ratio depth can be affected by electron trapping.

Fig. 1 shows an illustration of the four trapping cases considered in this paper. Case I is a normal pixel with 10% uniform bulk electron trapping along the whole depth under this pixel (the detector is placed with the anode at the top and the cathode at the bottom). Case II is a pixel with an electron-trapping defect at depth d_0 and all electrons under this pixel passing through this defect will be trapped by a certain percentage. Case III is a pixel with a severe electron trapping at depth d_0 that all electrons

Manuscript received November 15, 2003; revised April 25, 2004 and June 12, 2004. This work is supported by the DOE/NNSA NA-22 Office under Grant DE-FG03-01NN20122.

The authors are with the Department of Nuclear Engineering and Radiological Sciences, University of Michigan, Ann Arbor, MI 48109 USA (e-mail: zhangf@umich.edu).

Digital Object Identifier 10.1109/TNS.2004.839078

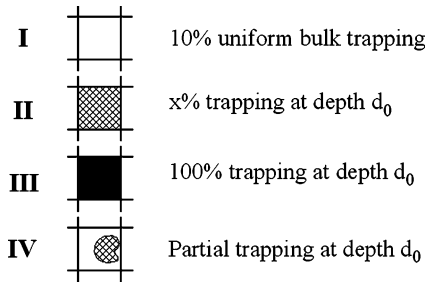

Fig. 1. Four pixels with different electron-trapping properties.

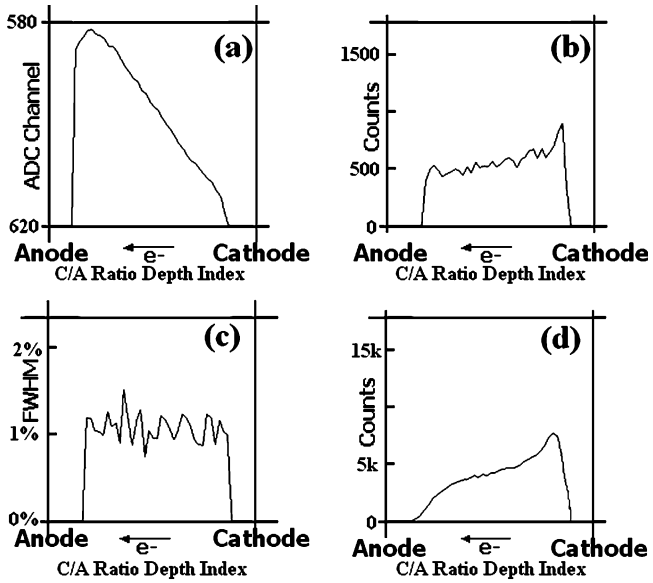

Fig. 2. Experimental results from one normal pixel, case I of Fig. 1. (a) Anode spectra photopeak centroid versus C/A ratio depth; please note that the y axis is offset from 0 and the actual change in the photopeak centroids is only $\sim$6%. (b) Photopeak counts versus C/A ratio depth. (c) Anode spectra FWHM at 662 keV versus C/A ratio depth. (d) Total counts versus C/A ratio depth.

will be trapped. Case IV is a pixel with an electron-trapping defect smaller than the pixel size at depth d_0. The experimental results from typical pixels of these four different trapping cases are presented in Fig. 2, Fig. 5, Fig. 6, and Fig. 7, respectively, and discussed in the following subsections.

A. Case I: 10% Uniform Bulk Trapping

In case I, because of the bulk electron trapping, the electrons will contribute to the cathode signal before they are trapped, while these trapped electrons will not contribute to the anode signal. Therefore, the C/A ratio will have a certain systematic shift over most of the interaction depth as discussed in [12]. However, the relation between the C/A ratio and the true depth should be linear over most of the interaction depth.

To observe the changes in the photopeak centroids, in the photopeak counts and in the total counts for different pixels and different interaction depths, an uncollimated 10 μCi ^{137}Cs source was placed 5 cm from the cathode surface. Sorted by the pixel location and the interaction depth derived from the C/A ratio, the collected single-pixel events were recorded in $\sim$4800 energy spectra for each voxel corresponding to a volume of $1.27 \times 1.27 \times 0.25$ mm within each detector. Since most voxel spectra have very sharp photopeaks ($\sim$1.0% FWHM at 662 keV), the 662-keV photopeak can be easily located, and the photopeak centroid, the energy resolution, the photopeak count, and the total count are measured for each voxel spectrum.

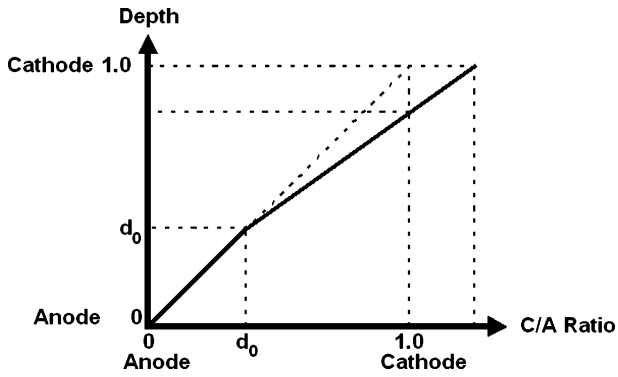

Fig. 3. Illustration of the relation between the true depth and the C/A ratio when there is a trapping defect.

As can be seen from Fig. 2(a), for normal pixels having no defects but only bulk electron trapping, the photopeak centroid decreases smoothly from the anode to the cathode due to uniform electron trapping. In Fig. 2(b) and (d), the decrease in the counts from the cathode side to the anode side is expected as discussed in [13], because the detectors were irradiated from the cathode side. The FWHM from all depths remains nearly unchanged despite some statistical fluctuation, as shown in Fig. 2(c).

B. Case II: x% Trapping Defect at Depth d_0

In case II, there is a trapping center at depth d_0 which traps x% of the electrons passing through it. Let us simplify the situation by not considering the bulk electron trapping and assuming ideal weighting potential that the weighting potential remains zero from the cathode surface ($d = 1$) to the anode ($d = 0$), then rises from zero to 1 on the anode surface. Then

$$\text{for } d < d_0, \quad \frac{C}{A} = \frac{d \times N_0 e}{N_0 e} = d \tag{1}$$

$$\begin{aligned}\text{for } d \geq d_0, \quad \frac{C}{A} &= \frac{(d-d_0)\times N_0 e + (1-x\%)\times N_0 e \times d_0}{(1-x\%)\times N_0 e} \\ &= \frac{d-d_0}{1-x\%} + d_0 \\ &= \frac{1}{1-x\%} \times d - \frac{x\%}{1-x\%} \times d_0. \end{aligned} \tag{2}$$

In the equations above, N_0 is the original number of electron-hole pairs created by the gamma-ray interaction, and d is the interaction depth.

As a result of (2), the C/A ratio between depth d_0 and the cathode will be larger than normal because the cathode signal is larger than the corresponding anode signal due to the electron-trapping defect at depth d_0, and those events close to the cathode will have a calculated C/A ratio even larger than 1.0, as we can see from Fig. 3. This change in the C/A ratio depth relation with the actual depth will affect the photopeak centroid and photopeak counts as a function of the C/A ratio depth.

As shown in Fig. 4(a), the relation between the normalized photopeak centroid as a function of the C/A ratio depth will have an abrupt change at the defect depth d_0. In the real data, this change may be smoothed out by other factors such as finite

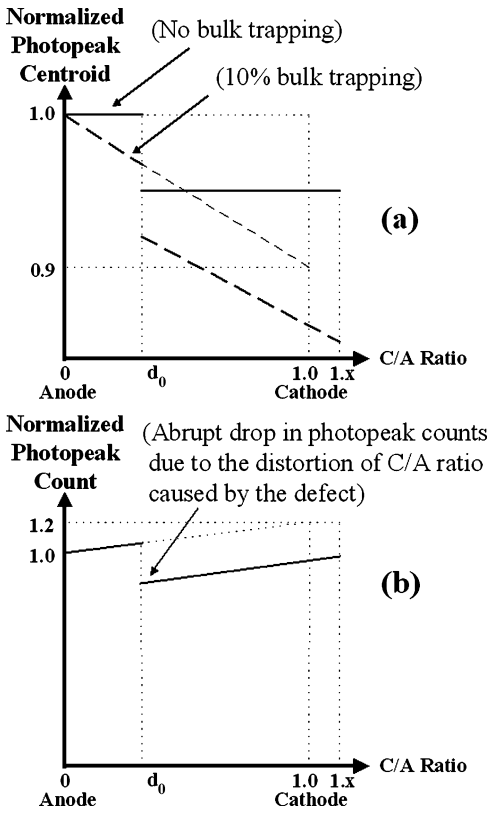

Fig. 4. If there is a trapping defect at depth d_0, (a) is the relation between the normalized photopeak centroid and the C/A ratio and (b) is the relation between the normalized photopeak counts and the C/A ratio.

depth resolution. But the change of slope in the relation is still present. If one still takes C/A ratio $= 1.0$ as the cathode and only selects the events with C/A ratio values varying from 0 to 1.0 for the electron-trapping analysis, the events from near the real cathode side $(1.0 - 1.x)$ are discarded. This results in underestimation in the calculated electron trapping.

Fig. 4(b) shows that the relation between the normalized photopeak counts versus the C/A ratio depth has an abrupt change and the photopeak counts between the cathode and the defect depth d_0 will be lower than what would be observed without the defect, because the thickness of the region between depth d_0 and the cathode derived from the C/A ratio $(d_0 - 1.0)$ is thinner than the thickness of the real depth region $(d_0 - 1.x)$.

Fig. 5 shows a pixel observed with such an electron-trapping defect at a certain depth. The change of slopes in the photopeak centroid versus the C/A ratio depth is not very prominent but still visible. The decreases in the photopeak counts, and in the total counts are quite clear. However, no significant degradation in the energy resolution can be observed.

C. Case III: 100% Trapping Defect at Depth d_0

In case III, if there is a severe electron-trapping defect at a certain depth under the pixel, all events that occur between this defect and the cathode cannot be recorded by the system. A pixel with such a defect is also observed and the photopeak centroids, the photopeak counts, the FWHM and the total counts are shown in Fig. 6.

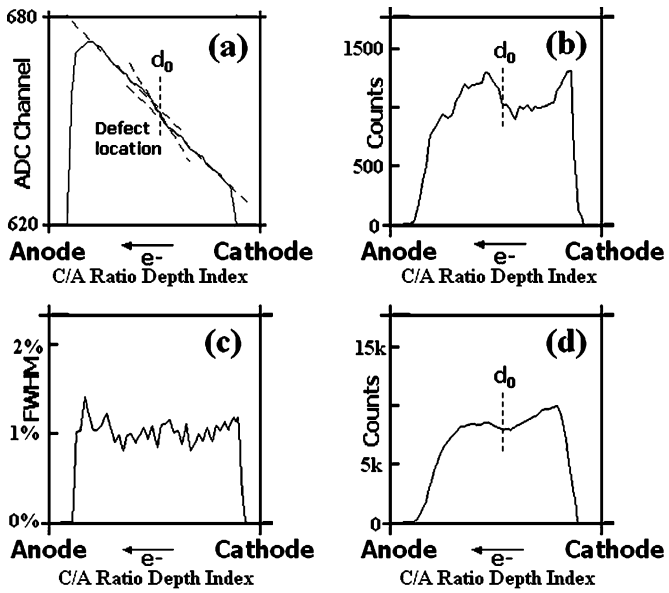

Fig. 5. Experimental results from one pixel with electron-trapping defect, case II of Fig. 1. (a) Anode spectra photopeak centroid versus C/A ratio depth. (b) Photopeak counts versus C/A ratio depth. (c) Anode spectra FWHM at 662 keV versus C/A ratio depth. (d) Total counts versus C/A ratio depth.

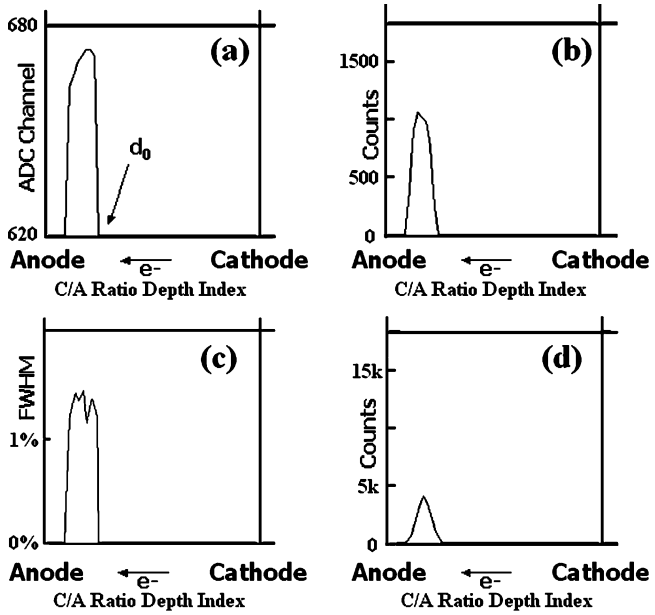

Fig. 6. Experimental results from one pixel with a defect that electrons cannot pass through, case III of Fig. 1. (a) Anode spectra photopeak centroid versus C/A ratio depth. (b) Photopeak counts versus C/A ratio depth. (c) Anode spectra FWHM at 662 keV versus C/A ratio depth. (d) Total counts versus C/A ratio depth.

D. Case IV: Trapping Defect Smaller Than the Pixel Size at Depth d_0

In case IV, if there is an electron-trapping defect smaller than the pixel size at depth d_0, only part of the events occurring between depth d_0 and the cathode are affected by this defect. The change in the C/A ratio should be somewhat between case I and case II, and the change in the photopeak centroids and the photopeak counts will not be as evident as in case II. However, the

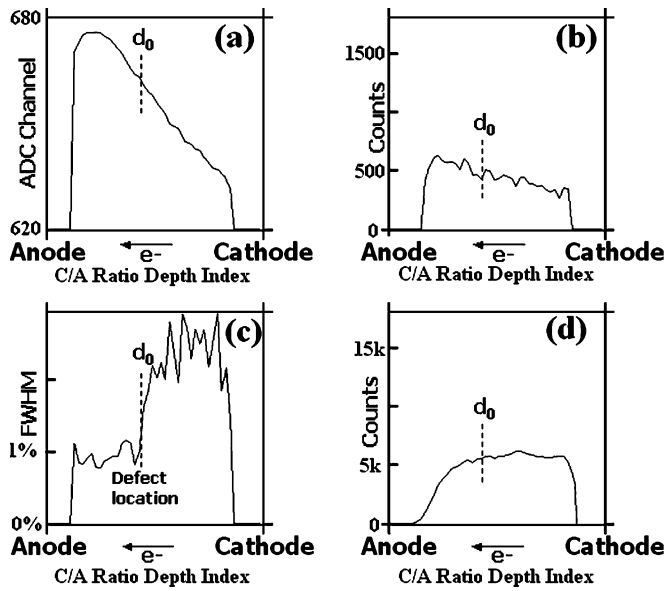

Fig. 7. Experimental results from one pixel with a small size electron-trapping defect, case IV of Fig. 1. (a) Anode spectra photopeak centroid versus C/A ratio depth. (b) Photopeak counts versus C/A ratio depth. (c) Anode spectra FWHM at 662 keV versus C/A ratio depth. (d) Total counts versus C/A ratio depth.

photopeaks between depth d_0 and the cathode will be broadened because some events will have electron trapping and some will not. As a result, the energy resolution will degrade after depth d_0, as shown in Fig. 7(c). Such a small electron-trapping defect can significantly degrade the energy resolution of the corresponding pixel. However, with 3-D position-sensing, those events affected by such a defect can be discarded.

Overall, for detector #2.2, we observed quite smooth and consistent relationship between the photopeak centroid and the C/A ratio depth, and the relationship between the electron drift time and the C/A ratio depth for most of the pixels. This result indicates that the material of this detector is quite uniform.

III. Variation of Ionization Energy

As we showed in (1) and (2) in the previous section, the C/A ratio is independent of the number of electrons generated and, thus, independent of the variation of ionization energy. If the ionization energy changes along the depth underneath one pixel, the C/A ratio will not be affected and thus the photopeak counts will not be affected. However, if the ionization energy varies at different locations within the crystal, the number of electrons generated by the deposited energy will vary, and the photopeak centroid may have nonsmooth shape if the ionization energy changes in a scale comparable to or larger than the scale of the depth resolution, as shown in Fig. 8(a). No such nonsmooth shape in the photopeak centroid plots was observed in either detector. If the ionization energy changes in a scale smaller than the depth resolution, we may observe worse energy resolution at certain depths, as shown in Fig. 8(b). Similarly, in the lateral direction, if the ionization energy changes in a scale comparable to or larger than the pixel size, we should observe large variations in the photopeak centroids among the pixels. If the ionization energy changes in a scale smaller than the pixel size, we should see worse energy resolution from the pixel.

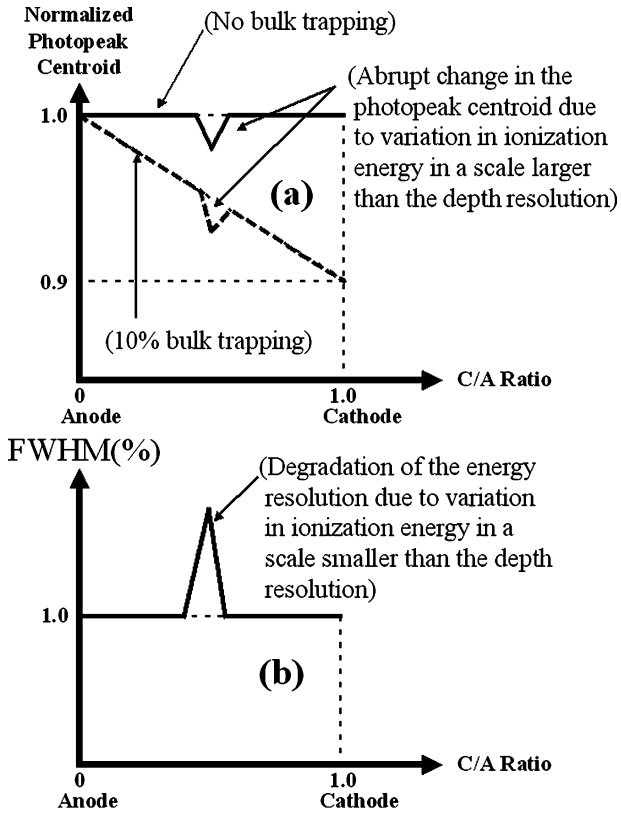

Fig. 8. Illustration of the effect of variation in ionization energy. (a) The scale of variation is comparable to the depth resolution. (b) The scale of variation is much smaller than the depth resolution.

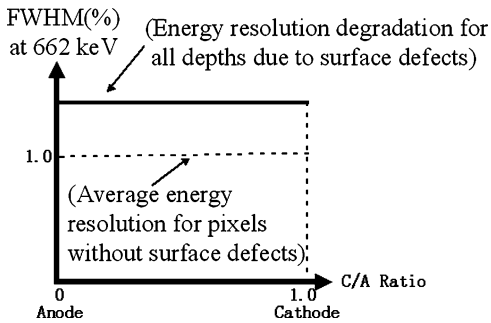

Fig. 9. Illustration of the degradation in energy resolution for all depths due to surface defect.

However, if there is a surface defect underneath the pixel anode, which affects the collection of electrons onto the pixel anode, the signal from all depths will be affected and have worse energy resolution at all depths as shown in Fig. 9. We cannot tell whether this degradation in energy resolution for all depths is due to the surface defect or due to the small-scale variation in ionization energy throughout all depths underneath this pixel as discussed in the previous paragraph and Fig. 8(b).

Such defects were observed in detector #2.3 (except Fig. 10, all other results in this paper are obtained from detector #2.2). As shown in Fig. 10(a), the pixels in the region marked by the dotted lines have smooth relation between the photopeak centroid and the C/A ratio depth, no abrupt change in the curve. This indicates there is no large-scale variation in ionization energy. However, these pixels have bad energy resolution for nearly all the depths, as can be seen in Fig. 10(b). This is either due

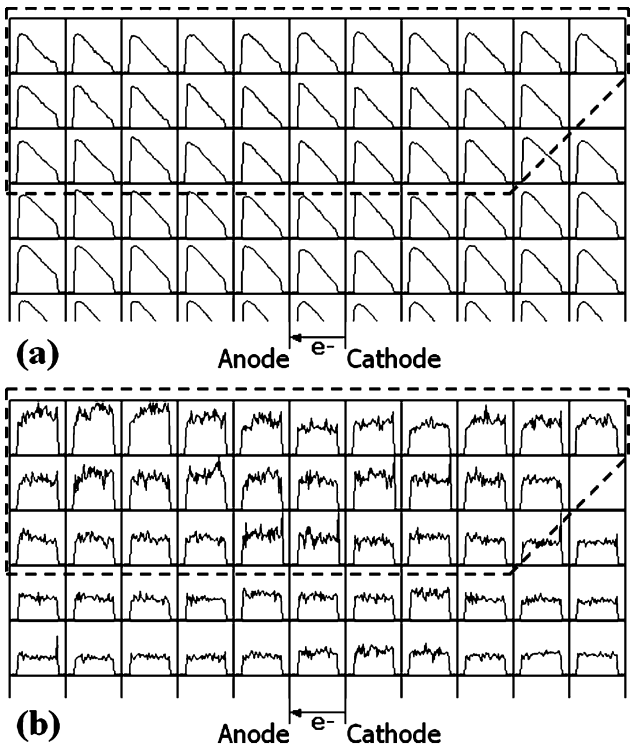

Fig. 10. Experimental results for upper half pixels on one detector, arranged in the geometrical location of the pixels on detector #2.3. For each pixel, the x axis is the C/A ratio depth index. (a) The relation between the anode photopeak centroid and the C/A ratio depth. For each pixel, the y axis is photopeak centroid measured in ADC channel (origin not at 0). (b) The relation between the anode FWHM (%) and the C/A ratio depth. For each pixel, the y axis is the energy resolution FWHM at 662 keV in units of percentage with a minimum at 0% and a maximum at 2.5%.

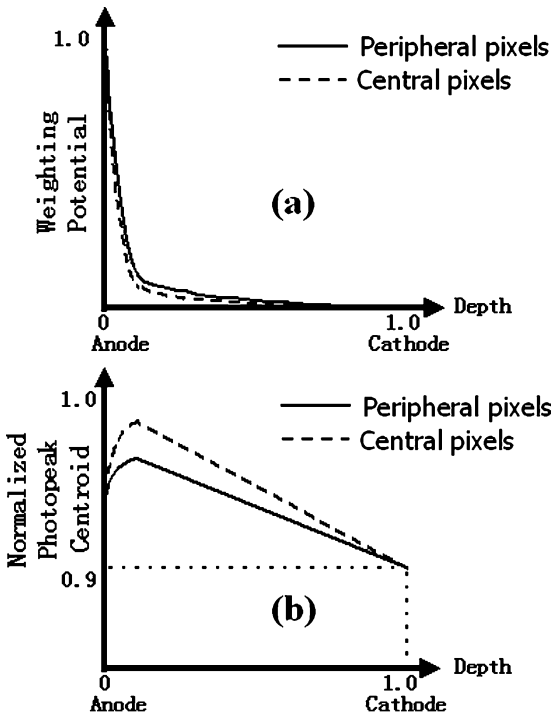

Fig. 11. Simulation results of the effect of weighting potential on edge pixels. (a) The relation between the normalized weighting potential and the normalized depth. (b) The relation between the normalized anode photopeak centroid and the normalized depth.

to surface defects or small-scale variation in ionization energy throughout all the depths under these pixels. Such performance degradation cannot be corrected even with 3-D position sensing. However, by discarding the events coming from the bad regions in the data processing and thus sacrificing the active detector volume, the good energy resolution of the good regions can still be retained.

For good pixels, the energy resolutions are around 1% for all the depths and the fluctuation of the FWHM is due to statistical variation. This shows that the bulk electron trapping/detrapping does not significantly degrade the energy resolution. Otherwise, the energy resolution should be worse on the cathode side because the electrons coming from the cathode side undergo more trapping/detrapping processes.

Since the electronic noise is around 6-keV FWHM and the energy resolutions for good pixels are around 7-keV FWHM for all depths, we can also draw a conclusion that the small scale variation in the ionization energy, if any, should not exceed 0.5% FWHM for those good pixels—$\sqrt{7^2 - 6^2}/662 \cong 0.5\%$.

IV. Weighting Potential

For pixels on the periphery and at corners of the anode surface, weighting potential is an important factor for the detector response. Due to the change in weighting potential for the pixels near the edge, the events coming from the anode side will have smaller signal than for central pixels, while the events coming from the cathode side remain the same, as can be seen in Fig. 11(a). As a result, the photopeak centroids shown in Fig. 11(b) seem to have smaller change from the anode to the cathode because the larger change in weighting potential (from the anode side to the cathode side) compensates the signal loss due to the electron trapping.

Since the amount of electron trapping is determined from the change in the photopeak centroid from the anode side to the cathode side, the smaller change in the photopeak centroid on peripheral pixels makes the calculated electron trapping smaller than it actually is. If the exponential relation of the electron trapping from the cathode to the anode side (excluding the region very close to the anode) is used to calculate the electron mobility-lifetime product [14], the $(\mu\tau)_e$ will be overestimated for the peripheral pixels, as can be seen in Fig. 12(a). Please note that the data for the pixels in the lower left corner is unreliable due to a major crystal defect in this region.

V. Variation in $(\mu\tau)_e$ and Energy Resolution

The statistical result of $(\mu\tau)_e$ shown in Fig. 12(b) was obtained from the 9×9 central pixels only, so that the overestimated $(\mu\tau)_e$ values of the peripheral pixels do not bias our results. The mean $(\mu\tau)_e$ value and its standard deviation are $5.3 \pm 0.54 \times 10^{-3}$ cm^2/V.

Because the whole detector thickness is divided into ~40 C/A ratio indexes, the transformation from the C/A ratio index into the true interaction depth could have up to 2.5% round-off error from discretizing, resulting in up to 2.5% systematic error in the measured $(\mu\tau)_e$. However, the relative standard deviation from the different pixels is ~10%, significantly larger than the measurement error (up to 2.5%). Therefore, the variation in the measured $(\mu\tau)_e$ from different pixels is likely due to the nonuniform

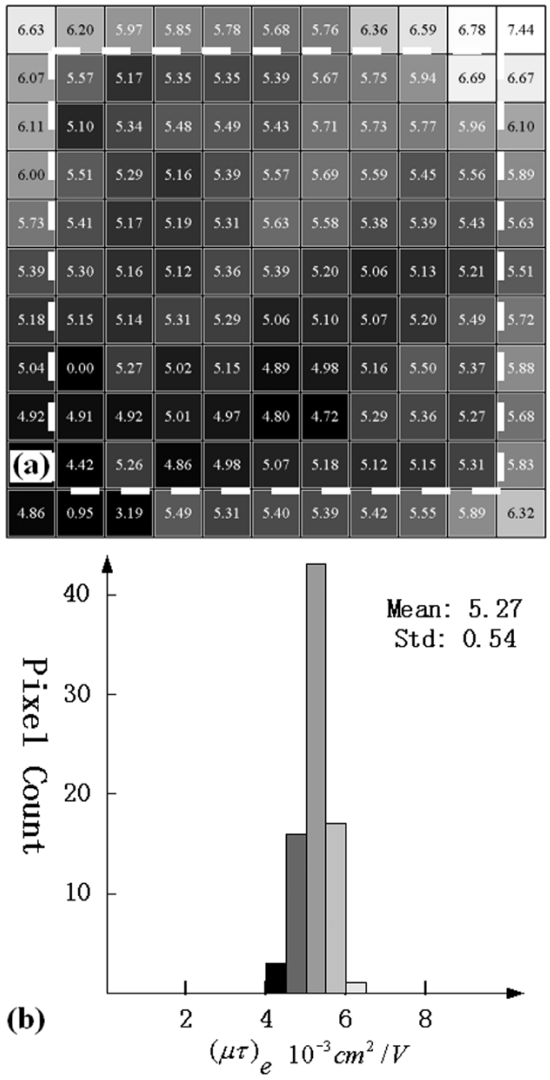

Fig. 12. Experimental results of the electron mobility-lifetime product (10^{-3} cm^2/V) for all the pixels of detector #2.2. (a) Pixel map of the $(\mu\tau)_e$ value. Darker color corresponds to lower $(\mu\tau)_e$. (b) Histogram of the $(\mu\tau)_e$ distribution for all the pixels.

electron trapping in the lateral dimension. Even with single polarity charge-sensing techniques and methods to compensate for electron trapping, such as relative gain [15] and depth sensing [10], the variations in $(\mu\tau)_e$ will result in variations in electron trapping and, thus, a broadening of the photopeak for events occurring at the same depths, but under pixels spread in the lateral direction. However, by doing 3-D correction of electron trapping, this variation can be mitigated to the size of the position resolution.

By comparing the $(\mu\tau)_e$ map shown in Fig. 12(a) and the energy resolution map shown in Fig. 13, no clear correlation between the $(\mu\tau)_e$ and the energy resolution can be found. It indicates that the bulk electron trapping is not the major reason for energy resolution degradation.

VI. Summary and Conclusion

Two $1.5 \times 1.5 \times 1.0$ cm^3 CdZnTe detectors (#2.2 and #2.3) constructed by eV-Products have been tested using VAS2/TAT2 ASICs. Gamma-ray spectra of a ^{137}Cs source

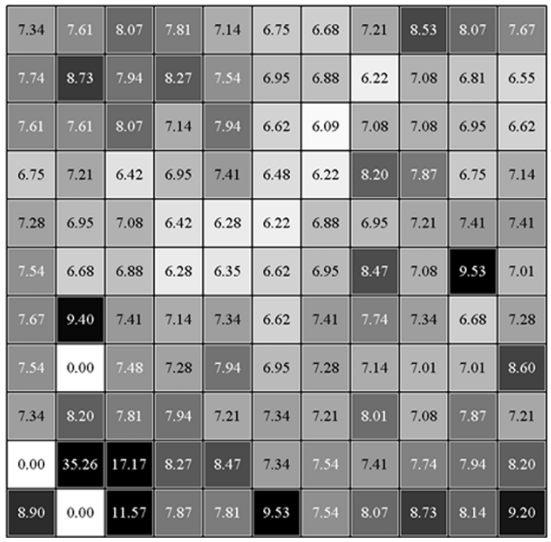

Fig. 13. Experimental results of the energy resolution FWHM (keV) at 662 keV for all the pixels (the spectra from all depths are aligned and combined for each pixel) of detector #2.2. Darker color corresponds to worse energy resolution.

were collected from ~4800 voxels of both detectors. This paper demonstrates that the detector response can be analyzed in 3-D using 3-D position-sensitive CdZnTe spectrometers. Variation in photopeak centroid, electron mobility-lifetime product, electron drift time, energy resolution, photopeak efficiency, and total efficiency in 3-D have been observed.

Possible effects of various electron-trapping defects, the variation in ionization energy, any surface defects, and the variation in weighting potential have been discussed. The 3-D detector response can be used to identify possible defects in the detector. The experimental results show that large lateral size electron-trapping defects do not significantly degrade the energy resolution of the corresponding pixels, but small ones do. However, with 3-D position sensing, the events coming from the bad region can be discarded. It has also been discussed that the small-scale variation in the ionization energy, if any, should not exceed 0.5% FWHM for most pixels.

It has been shown that bulk electron trapping/detrapping does not significantly degrade the energy resolution with the help of the 3-D position sensing and correction. No clear correlation between $(\mu\tau)_e$ and energy resolution was observed in these detectors.

Detector #2.2 has good uniformity over most of the volume, while detector #2.3 has possible surface defects or small-scale ionization energy variation in one-fourth region of the volume. Both detectors have achieved good energy resolution (close to 1.1% FWHM at 662 keV) after correction for 3-D detector response. The variation in electron trapping in lateral direction has been observed and the advantage of 3-D position sensing, especially in reducing the impact of material nonuniformity has been discussed.

References

[1] Z. He, W. Li, G. F. Knoll, D. K. Wehe, J. E. Berry, and C. M. Stahle, "3-D position sensitive CdZnTe gamma-ray spectrometers," *Nucl. Instrum. Methods A*, vol. 422, pp. 173–178, 1999.

[2] W. Li, Z. He, G. F. Knoll, D. K. Wehe, and J. E. Berry, "A data acquisition and processing system for 3-D position sensitive CZT gamma-ray spectrometers," *IEEE Trans. Nucl. Sci.*, vol. 46, pp. 1989–1994, Dec. 1999.
[3] VAS-TAT ASIC development, Univ. Michigan and Ideas ASA, Norway. 1998–2003. Internal reports.
[4] W. Li, "Three-dimensional position sensitive CdZnTe gamma ray spectrometers," Ph.D. dissertation, Univ. Michigan, Ann Arbor, MI, 2001.
[5] J. L. Matteson, M. R. Pelling, and R. T. Skelton, "CZT detectors with 3-D readout for gamma-ray spectroscopy and imaging," *Proc. SPIE*, vol. 4784, pp. 1–13, 2002.
[6] F. Zhang, Z. He, D. Xu, G. F. Knoll, D. K. Wehe, and J. E. Berry, "Improved resolution for 3-D position sensitive CdZnTe spectrometers," *IEEE Trans. Nucl. Sci.*, to be published.
[7] eV-Prodcuts, Saxonburg, PA.
[8] Ideas ASA, Snarøya, Norway.
[9] Z. He, G. F. Knoll, D. K. Wehe, R. Rojeski, C. H. Mastrangelo, M. Hammig, C. Barrett, and A. Uritani, "1-D position sensitive single carrier semiconductor detectors," *Nucl. Instrum. Methods A*, vol. 380, pp. 228–231, 1996.
[10] Z. He, G. F. Knoll, D. K. Wehe, and J. Miyamoto, "Position-sensitive single carrier CdZnTe detectors," *Nucl. Instrum. Methods A*, vol. 388, pp. 180–185, 1997.
[11] H. H. Barrett, J. D. Eskin, and H. B. Barber, "Charge transport in arrays of semiconductor gamma-ray detectors," *Phys. Rev.*, vol. 75, pp. 156–159, 1995.
[12] W. Li, Z. He, G. F. Knoll, D. K. Wehe, and Y. F. Du, "A modeling method to calibrate the interaction depth in 3-D position sensitive CdZnTe gamma-ray spectrometers," *IEEE Trans. Nucl. Sci.*, vol. 47, pp. 890–894, June 2000.
[13] W. Li, Z. He, G. F. Knoll, D. K. Wehe, and C. M. Stahle, "Spatial variation of energy resolution in 3-D position sensitive CZT gamma-ray spectrometers," *IEEE Trans. Nucl. Sci.*, vol. 46, pp. 187–192, June 1999.
[14] Z. He, W. Li, G. F. Knoll, D. K. Wehe, and C. M. Stahle, "Measurement of material uniformity using 3-D position sensitive CdZnTe gamma-ray spectrometers," *Nucl. Instrum. Methods A*, vol. 441, pp. 459–467, 2000.
[15] P. N. Luke, "Unipolar charge sensing with coplanar electrodes-application to semiconductor detectors," *IEEE Trans. Nucl. Sci.*, vol. 42, pp. 207–213, Aug. 1995.